DESIGN AND EXPERIMENT OF A MULTI-CHANNEL REAL-TIME WEIGHING DEVICE
/
多路实时称量装置设计与试验

Lingyu LIU, Xiangcai ZHANG*), Xianliang WANG, Zhongcai WEI, Xiupei CHENG, Yujie ZHANG, Xinkai JIAO [1]
School of Agricultural Engineering and Food Science, Shandong University of Technology, Zibo (255000), China
Tel: +86-15169235925; E-mail: zxcai0216@163.com
Corresponding author: Xiangcai Zhang
DOI: https://doi.org/10.35633/inmateh-73-28

Keywords: *seeding rate detection, SPI, pressure sensors, LabVIEW upper computer, DEM*

ABSTRACT

During the sowing operation, the consistency and stability of the row dispenses of a seeder are important indicators for evaluating sowing performance. A multi-channel real-time weighing device was designed to study and analyze the consistency of row dispenses in seeder under identical conditions, as well as the stability of dispenses from a seed dispenser. This device utilized two Arduino boards as controllers for data acquisition, processing, and transmission. Based on the Serial Peripheral Interface (SPI), data exchange between multiple Arduinos was achieved in a master-slave configuration, allowing for data acquisition from 14 pressure sensors in a one-master, one-slave setup. Pressure data was collected using pressure sensors, HX711 converter chips, and Arduino. LabVIEW was utilized as the upper computer to read data from the Arduino host serial port and provide real-time display and storage. This paper presents the structural and working principles of the device. Experimental tests on the weighing unit were conducted using a test bench to evaluate measurement errors. The absolute error mean ranged from 0.143 g to 0.262 g. Additionally, the impact of the seed impact force on the error was simulated using EDEM. The device was used to evaluate a six-row wheat seeder under the experimental conditions of the groove wheel having a length of 2.5 cm and a groove wheel speed of 25 r/min. The maximum coefficient of variation for seeding stability (Y_1) was 2.38%, the minimum was 0.83%, and the mean was 1.21%. The coefficient of variation for consistency of seeding in rows (Y_2) was 1.86%.

摘要

在进行播种作业时，播种机的各行排量一致性和排量稳定性是评价播种性能的重要指标。为了研究和分析在相同条件下，同一播种机的各行排量一致性，以及单一排种器的排量稳定性，设计了一种多路实时称量装置。该装置以两块 Arduino UNO 作为控制器，用于装置数据的采集、处理和传输；基于 SPI 通信原理，实现多 Arduino 的主从机数据交换，一主一从时，可实现 14 个压力传感器的数据采集；通过应变式压力传感器、HX711 A/D 转换器芯片和 Arduino 实现压力数据采集；应用 LabVIEW 上位机用于读取 Arduino 主机串口的数据，并进行实时显示和存储。本文介绍了该装置的结构构成以及工作原理，通过台架试验，检验了称重单体的测量误差，并对误差做出了分析，绝对误差均值在 0.143g 至 0.262g 之间，并通过 EDEM 离散元仿真模拟了种子冲击力大小对误差的影响。运用该装置检验了 6 行单箱小麦播种机在外槽轮开度 2.5cm、槽轮转速 25r/min 的试验条件下，排量稳定性变异系数最大值为 2.38%，最小值为 0.83%，均值为 1.21%，各行排量一致性变异系数为 1.86%。

INTRODUCTION

With the development of precision agriculture, seeding detection technology is gradually becoming one of the research hotspots to achieve intelligent seeding, providing essential technical support to enhance seeding quality *(Ding et al., 2021; He et al., 2021; Ramasamy, 2021)*. Improving seeding uniformity to ensure crop seedlings are uniform and strong can provide favorable conditions for crop growth, laying a foundation for increasing yields in the early stages *(Wang et al., 2024)*.

Since the 1980s, research on seeding detection technology has been carried out both domestically and internationally *(Li et al., 2022)*. In the early stages, mechanical alarms were used, such as on the NODET air-suction seeder developed in France *(Zhao et al., 2003)*, where an actively fitted spring plate would strike a raised shield to trigger an alarm using metal components but could only determine the working status of the seeder.

[1] *Lingyu Liu, M.Sc. Stud. Eng.; Xiangcai Zhang, Ph.D. Eng.; Xianliang Wang, Ph.D. Eng.; Zhongcai Wei, Ph.D. Eng.; Xiupei Cheng, Ph.D. Eng.; Yujie Zhang, M.Sc. Stud. Eng.; Xinkai Jiao, M.Sc. Stud. Eng.*

Based on the sensing principles of different detection devices for seeds, the existing detection methods mainly include mechanical-electrical, machine vision, photoelectric sensing, capacitive sensing *(Taghinezhad et al., 2013)*, and piezoelectric sensing (*Sebastián Rossi et al., 2023*). *Drake et al. (1991)* combined high-speed photography with image processing technology to measure and analyze the motion of seeds falling from the seed outlet. *Zhang et al. (2013)* used red high-brightness light-emitting diodes in conjunction with a photoresistor as the sensing component for seeds, coupled with a microcontroller, to design a photoelectric seed and fertilizer detection system. *Wu et al. (2014)* used pressure sensors to monitor the real-time changes in the mass of the seed box and provide feedback to adjust the seeder's speed to control the seeding quantity. This enables the detection of key information such as blockages, seeding quantity, seeding frequency, misplanting, overplanting, and seed motion status *(Karimi et al., 2017; Zhang et al., 2022; Zhou et al., 2022)*. However, there is a lack of a detection device specifically for detecting the consistency of seeding quantities in each row of seeders, and existing seeding detection devices developed domestically and internationally suffer from issues such as single application, limited detection channels that are difficult to install and dismantle, poor environmental adaptability, high costs, and a lack of mature technical systems and marketable products *(Li & Yang, 2018; Wang et al., 2021; Zhang et al., 2021; Zagainov Nikolay et al., 2023)*.

To address this, research was conducted on aspects such as the structure of the weighing unit, operational principles, error analysis, and upper and lower machine program design. The weighing device was designed and characterized by its multi-channel, real-time display and synchronous operation. This device provides technical and data support for assessing the consistency and stability of the row dispenses of a seeder and also serves as a foundational reference for the design of other agricultural machinery in areas such as broadcast sowing, row sowing, and irrigation.

MATERIALS AND METHODS

General structure and working principle

The overall schematic diagram of the multi-channel real-time weighing device is illustrated in Fig. 1, which is comprised mainly of the LabVIEW upper computer, Arduino master, Arduino slave, weighing unit, and Serial Peripheral Interface (SPI) communication system. The LabVIEW upper computer, Arduino master, and Arduino slave adopt a three-tier distributed structure.

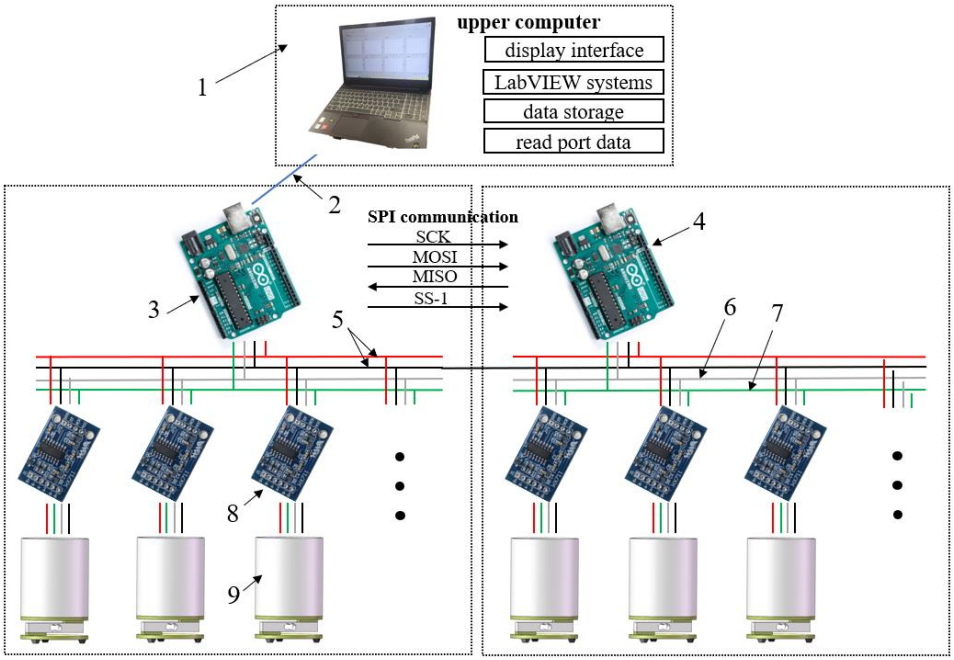

Fig. 1 - The overall schematic diagram of the device

1 – LabVIEW upper computer; 2 – Type-B to Type-A; 3 – Arduino master; 4 – Arduino slave; 5 – 5v power supply; 6 – SCK cord; 7 – DT cord; 8 – HX711 converter chip; 9 – weighing unit

The multi-channel real-time weighing device was designed with a master unit and a slave unit, comprising 8 weighing units (theoretically expandable up to 14), capable of simultaneously conducting real-time monitoring of 8 targets. Each weighing unit was primarily composed of a pressure sensor and a weighing cylinder, which function to acquire the weight of the target and output its mass.

The Arduino master unit is responsible for collecting real-time data from its own weighing units, selecting the communication slave unit, collecting real-time data from the slave unit weighing units, integrating all the data, and printing it via the serial port. The Arduino slave unit was tasked with collecting real-time data from its own weighing units and transmitting the data to the master unit upon selection. SPI communication was employed for the Arduino master unit to select the Arduino slave unit and perform data exchange. The LabVIEW control system runs on a computer equipped with LabVIEW 2018 software. Through LabVIEW software programming, it reads, separates, displays, and stores data from the Arduino master unit via the serial port. During operation, each weighing unit was placed beneath the weighing target, and the target continuously enters each weighing unit, enabling multi-channel real-time weighing.

Weighing unit structure

The schematic diagram of the weighing unit structure is shown in Fig. 2. The weighing unit is one of the main functional components of the multi-channel real-time weighing device, designed to acquire the weighing target and output the target's mass. It primarily consists of a weighing cylinder, upper fixed plate, strain gauge pressure sensor, spacer, HX711 converter chip, lower fixed plate, and foot pad. During operation, the unit remained in a static state.

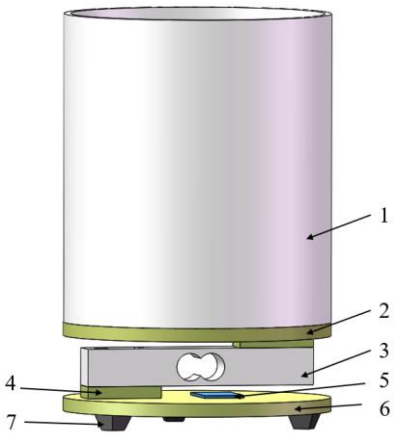

Fig. 2 - The schematic diagram of the weighing unit structure

1 – weighing cylinder; 2 – upper fixed plate; 3 – strain gauge pressure sensor; 4 – spacer; 5 – HX711 converter chip; 6 – lower fixed plate; 7 – foot pad

In Fig. 2, both the upper fixed plate and lower fixed plate are made of acrylic plates. Three rubber foot pads are fixed to the lower surface of the lower fixed plate to provide support and stability to the entire working component. The HX711 converter chip is secured to the upper surface of the lower fixed plate by two rivets, positioned closely to the pressure sensor without affecting signal transmission. According to the working principle of the strain gauge pressure sensor, the lower left and upper right ends of the pressure sensor are respectively fixed to the lower fixed plate and upper fixed plate through acrylic spacers and bolts. The weighing cylinder is fixed to the upper surface of the upper fixed plate with two bolts, serving to support the seeds discharged by a single seed dispenser.

Principles of data acquisition

The data acquisition of this device primarily consists of a strain gauge pressure sensor, an HX711 converter chip, and an Arduino board. A 5 kg range pressure sensor was selected to meet the test requirements of *GB/T 9478-2005* for grain strip planter testing methods. The pressure sensor is used to sense external pressure changes and generate corresponding voltage signals for output to the HX711 converter chip. The strain gauge pressure sensor is an elongated prism-shaped elastic element with a hollow center that undergoes slight elastic deformation when force is applied. There is a strain gauge on each of its upper and lower surfaces, with two pressure resistors within each strain gauge. When the elastic element deforms due to force, the upper strain gauge experiences tension while the lower strain gauge undergoes compression, and causing a change in resistance in the resistive wire leading to an imbalance in the original bridge configuration. The four pressure resistors form a full bridge circuit, enhancing measurement accuracy *(Ghanbari & Rezazad, 2022; Gu et al., 2024)*. The operational principle is depicted in Fig. 3. In the process of connecting the four lead wires of the pressure sensor to the HX711 converter chip, the black wire connects to *E-*, the white wire connects to *S-A*, the red wire connects to *E+*, and the green wire connects to *S+A*.

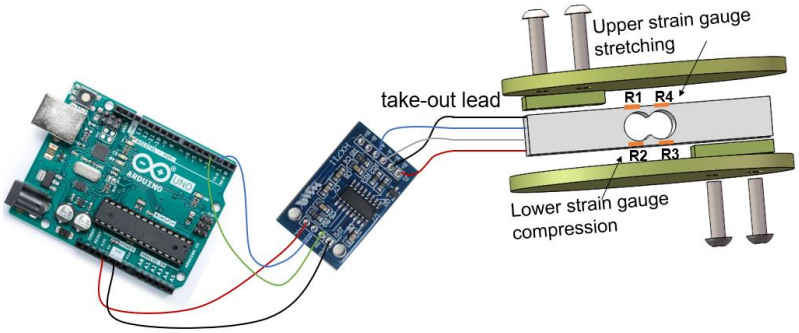

Fig. 3 - Strain gauge pressure sensor working principle diagram

The HX711 is a 24-bit A/D converter chip specifically designed for high-precision weighing sensors. In comparison to similar chips, the HX711 integrates features such as a stable power supply and an on-chip clock oscillator, eliminating the need for external peripheral circuits required by other chips of the same type. It is characterized by high integration, fast response speed, and strong anti-interference capability, which not only saves costs but also enhances the performance and reliability of the entire system. The main function of the HX711 is to amplify the voltage signal generated by the pressure sensor and convert the voltage signal into a digital signal. In this device, the A channel of the HX711 with a 128-gain is utilized, and the analog differential input of HX711 Channel A can be directly connected to the differential output of the pressure sensor. To fully utilize the input dynamic range of the A/D converter, it is necessary to amplify the relatively small voltage signal generated by the bridge sensor, and then the on-chip A/D converter will convert the voltage signal into a digital signal for output.

This device utilizes two Arduino boards to read the digital signals output by multiple HX711 converter chips and performs calculations with the intermediate value *GapValue* to determine the mass of the heavy object. The system frequency was set at 9600 for both boards, with one serving as the master to read data from the sensors to which it is connected. The master simultaneously selects the slave, receives data from the sensors connected to the slave, and prints the data on the master's serial port. The second board functions as the slave, reading data from its own connected sensors. When selected by the master board to establish communication, it transmits the collected data to the master board.

The *GapValue* is an intermediary variable used in the calculation of the mass of the heavy object. By adjusting its value, the pressure sensor can be calibrated.

The formula for calculating the mass of the heavy object is Eq. 1.

$$M=\frac{D}{GapValue} \tag{1}$$

where: M is the mass of the heavy object. D is Sensor reading. *GapValue* is intermediary variable.

$$GapValue=\frac{X\cdot 0.86\cdot 2^{24}}{4.3} \tag{2}$$

where: X is magnifying power.

Due to the varying slope characteristics of different pressure sensors, the *GapValue* calculated by the formula represents the theoretical value, and actual calibration of each pressure sensor is required. In order to improve computational speed and reduce storage space resource usage, many programs scale the received AD sample values during data processing, resulting in the loss of lower-order data bits. As a result, the measurement accuracy of the program is around 1 g. By not scaling the data, reducing the *GapValue* value by a factor of 100, and dividing the output data by 100, the output mass results can retain two decimal places.

Due to the limited volume of the weighing cylinder during operation, in order to improve the accuracy of the data for this experiment, calibration was performed using a 1 kg standard weight. The calibration procedure involves burning the program onto the Arduino board with no weight on the pressure sensor, opening the serial monitor, and observing an initial reading of 0 g. The 1000 g standard weight was then placed on the pressure sensor, and the displayed value on the serial monitor is observed. If the value was higher than expected, the *GapValue* was increased and the Arduino program is re-burned. If the value is lower, the *GapValue* was decreased. This process was repeated multiple times until the value is accurate, indicating successful calibration. The *GapValue* values for each sensor are provided in Table 1.

Table 1

The *GapValue* values for each sensor

Number	1	2	3	4	5	6	7	8
Value	4.30	4.29	4.21	4.25	4.30	4.28	4.15	4.16

Principles of SPI

In order to collect data from multiple sensors and achieve modularity in the system, the Serial Peripheral Interface (SPI) was adopted. SPI is a high-speed, full-duplex, synchronous communication bus. SPI operates in a master-slave configuration, allowing one master device to communicate with multiple slave devices. The master device selects different slave devices for communication using separate SS/CS signal lines and performs bidirectional data exchange under the control of the SCK (serial clock) signal *(Yang & Ding, 2012)*.

The system consists of one master and one slave board, with a bus utilizing four data lines for data transfer. These lines are connected through pins 10, 11, 12, and 13 of the Arduino UNO, serving as the control signal line SS-1 (slave select), the data signal line MOSI (master out slave in), the data signal line MISO (master in slave out), and the control signal line SCK for communication. To ensure the stability of the communication process, the GND(Ground) pins of the master and slave devices are connected. To guarantee the stability of data transmission in SPI communication, the communication clock starts with a 2x clock division, and eventually, the communication clock for the multi-channel real-time weighing device was set to SPI_CLOCK_DIV16 to define it as one-sixteenth of the system clock frequency.

During communication, the master initiates SPI by setting the SS-1 pin of the slave device to a low logic level, selecting the desired slave for communication. The selected slave board detects the initiation, establishes communication, and data is synchronously exchanged between the master and slave boards during the communication process. When the master detects the transmission of the "p" character from the slave device, it concludes one communication session by setting the SS-1 pin of the slave device to a high logic level, deselecting the slave. The slave device then disregards the host, and when not selected, the MOSI signal line remains in a high impedance state, awaiting the next communication session with the host.

Principles of LabVIEW

LabVIEW is a graphical development environment language that provides the necessary development environment for various applications such as data acquisition, instrument control, measurement analysis, and data display *(Gong & Zhang, 2020)*. Upon the initialization of LabVIEW software, this device configured the serial port using VISA, initialized the selected serial port at a communication frequency of 9600, and set the VISA resource name as "Arduino master serial port.". Serial port data was read, and a regular expression is used to search for the presence of the character "p" in the input string, which is then split into sub-strings. After splitting, the sub-strings are converted into numerical values, placed in an array, and displayed on the front panel. By indexing the array, the variation of individual sensor data curves is displayed in real-time on the front panel of the software. Simultaneously, utilizing file writing functionality to store the data from each sensor in a local folder on the computer, for subsequent data processing and analysis. The LabVIEW front panel interface is shown in Fig. 4, and the overall workflow of the LabVIEW system is depicted in Fig. 5.

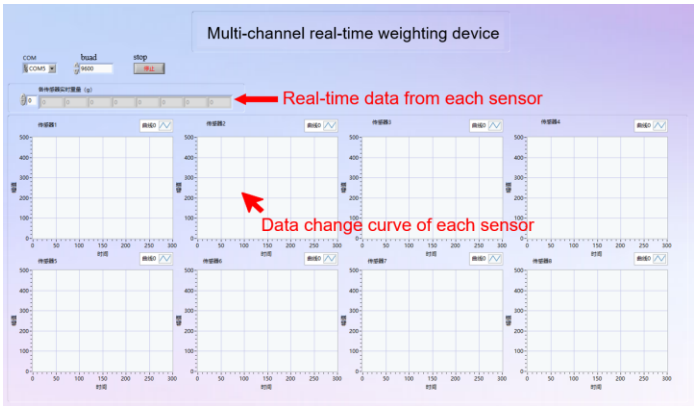

Fig. 4 - The LabVIEW front panel interface

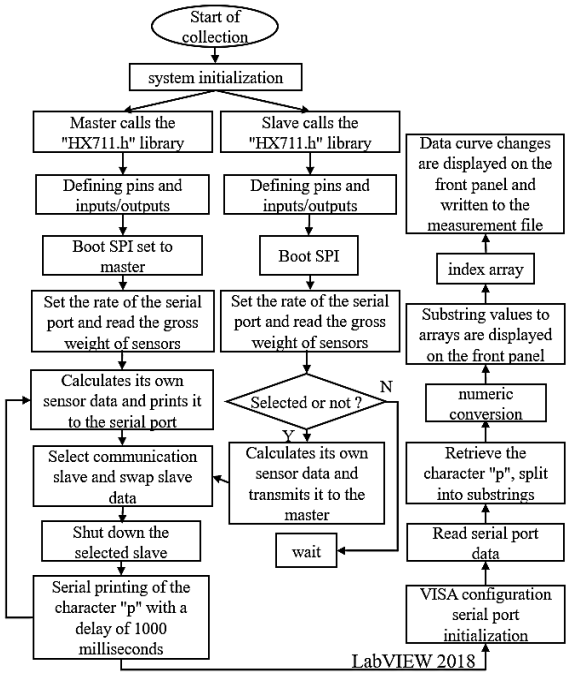

Fig. 5 - Overall workflow of the LabVIEW system

Principles of circuit

The hardware circuit connections of the device primarily consist of a pressure sensor, HX711 conversion chip, and Arduino board forming the signal processing circuit, as well as the SPI communication circuit for communication between the Arduino master and slave. The schematic diagram of the device circuit is shown in Fig. 6.

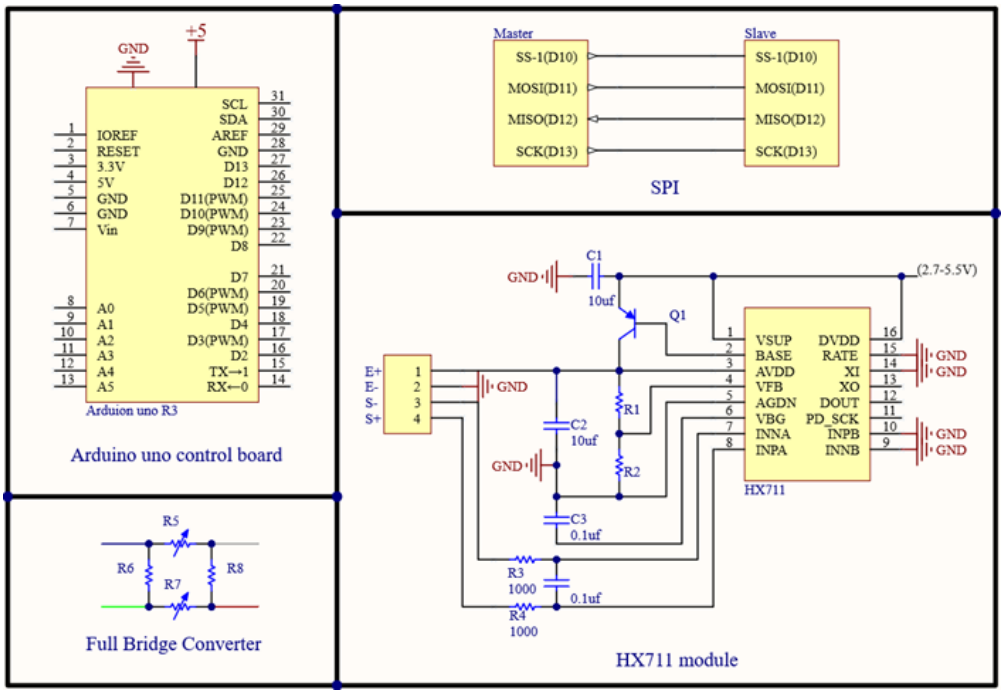

Fig. 6 - The schematic diagram of the device circuit

The Arduino master and slave can each connect up to seven strain gauge pressure sensors. In this design, four strain gauge pressure sensors are connected to both the master and slave Arduino boards. When connecting the HX711 conversion chip to the Arduino board, it is necessary to define the pins on the Arduino board. The VCC of the HX711 was connected to the 5V power output of the Arduino board, and the GND was connected to the GND pin of the Arduino board. The 2, 4, 6, and 8 pins of the Arduino master and slave were defined as output ports and connected to the SCK output pulses of each HX711. The 3, 5, 7, and 9 pins of the Arduino master and slave were defined as input ports and connected to the DT for data reading from each HX711. The 10, 11, 12, and 13 pins of the Arduino master and slave were defined and connected for SPI communication. The Arduino master was connected to the LabVIEW upper computer via a Type-B to Type-A cable.

Bench test error measurements method

In order to analyze the error between the measured values and the true values of the pressure sensor during operation, a bench test experiment was designed, as shown in Fig. 7. The row seeder of a wheat seed dispenser with external groove wheel was fixed on the bench, with a seed box mounted above the seeder. A weighing unit was placed 20 cm below the seeder outlet, driven by a stepper motor to rotate the seed dispenser with a groove wheel. The groove wheel has a length of 2.5 cm and the groove wheel speed of 25 r min^{-1}. The seed box was filled with wheat seeds, and the stepper motor was activated to start seeding. The seeds fell into the weighing cylinder underneath the working part in sequence. After rotating the stepper motor for two full rotations, it was stopped. The maximum value measured by the weighing unit at the end of seeding was taken as the measured value. The mass of the discharged seeds was measured using a high-precision balance with a precision of one thousandth as the true value. Absolute error and relative error analyses were conducted based on the measured values from the weighing unit and the true values from the high-precision balance. Each test was repeated three times to take the average value. The seeds in the weighting cylinder were then emptied, and the stepper motor was set to rotate for 4 full rotations before stopping, and the above test was repeated. The experiment was conducted by incrementing 2 rotations each time until the stepper motor completed 20 rotations, totaling 10 sets of experiments.

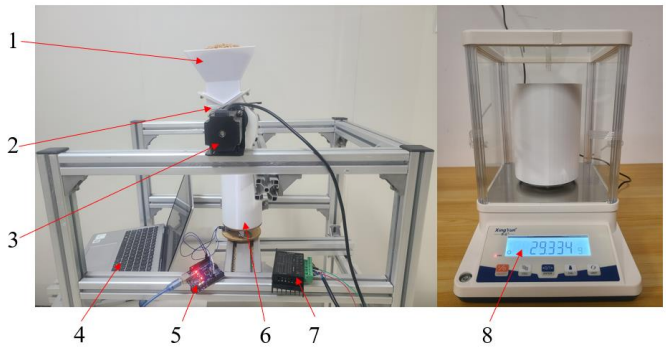

Fig. 7 - The bench test experiment

1 – seed box; 2 – seed dispenser with external groove wheel; 3 – stepper motor; 4 – computer; 5 – Arduino board; 6 – weighting unit; 7 – motor controller; 8 – high-precision balance; 9 – weighing unit

Impact error simulation method

When wheat seed is discharged from the seed dispenser, it acquires an initial velocity (v_a) and collides with the bottom of the weighing cylinder after falling a height (h), generating an impact force (P) at the moment of collision. The schematic diagram of the seed collision motion is shown in Fig. 8. Due to the random direction of the wheat seeds during descent and their irregular shapes, the direction of the impact force when they collide with the bottom of the weighing cylinder is also not fixed. The impact force direction is always perpendicular to the contact surface between the wheat seed and the bottom of the weighing cylinder. If the seed is considered a particle, the motion equation when it falls to a height (h) can be expressed as:

$$h=v_a \cdot t+\frac{1}{2}gt^2 \tag{3}$$

where: v_a is initial velocity of wheat seeds (m/s); g is the gravitational acceleration

The time t for the seed to fall is:

$$t=\frac{-v_a+\sqrt{v_a^2-2gh}}{g} \tag{4}$$

where: h is seed drop height (m).

During the impact process considered as a point particle, there exists a gravitational force (G) and a normal pressure (P) acting on the particle. According to the principle of kinetic energy:

$$\frac{1}{2}mv_a^2+G(t+t_1)=P \cdot t_1 \tag{5}$$

where: t_1 is normal pressure action time (s).

Bringing the time t into Eq. (5) yields:

$$P=\frac{mv_a^2}{2t_1}+mg\left(\frac{-v_a+\sqrt{v_a^2-2gh}}{t_1 g}+1\right) \tag{6}$$

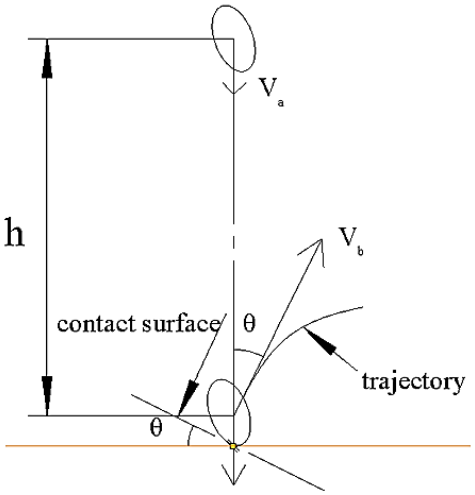

Fig. 8 - The schematic diagram of the seed collision motion

From Eq. (6), it can be observed that, with other conditions remaining constant, the impact force increases as the duration (t_1) of positive pressure decreases or as the height (h) of seed descent increases. In order to measure and analyze the impact of the impact force (P) on the pressure sensor reading during collision, EDEM discrete element simulation experiments were conducted. To simplify the calculation process, based on the measurement of the physical properties of Jima 22 seeds and references from literature, wheat seeds were equivalently modeled as ellipsoidal particles using five spherical particles. The model had a major axis length of 6.49 mm and minor axis length of 3.3 mm. The particle model is shown in Fig. 9, and the key parameters *(Yu et al., 2018; Yu et al., 2020)* for seed-DEM simulation are presented in Table 2.

Table 2

Basic parameters of seed and discrete element models

Parameters	Value
seed triaxial size (mm×mm×mm)	6.49×3.36×3.05
seed Poisson's ratio	0.434
seed shear modulus (Pa)	5.24×10^{7}
seed density (kg/m^3)	1223
ABS Plastic Poisson's ratio	0.6
ABS Plastic shear modulus (Pa)	8.96×10^{8}
ABS Plastic density (kg/m^2)	1060
seed-to-seed collision coefficient	0.407
coefficient of static friction between seeds	0.523
coefficient of kinetic friction between seeds	0.082
seed - ABS collision coefficient	0.507
seed - ABS static friction coefficient	0.563
seed - ABS coefficient of kinetic friction	0.051

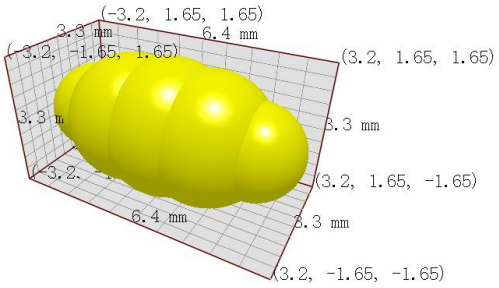

Fig. 9 - Particle model

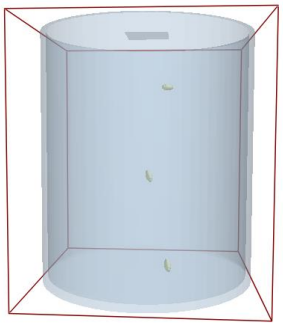

Fig. 10 - Simulation

Using SolidWorks 2016 modeling software, a three-dimensional model of the weighing cylinder component was created and then imported into the EDEM environment in *.igs* format for analysis. The simulation employed the default Hertz-Mindlin non-sliding contact model to analyze the impact force of wheat seed. A grain factory was established 115 mm directly above the weighing cylinder, and at the start of the simulation, seed particles were created with a velocity of 1.5 m/s along the negative Y-axis. To capture more data points and accurately reflect the collision process, the simulation was paused near the collision, and the time step was set to 10% of the Rayleigh Time Step. Data was stored at intervals of 1×10^{-5}s before continuing the simulation. During playback of the animation, it was observed that the positions of the seed before and after collision were continuous. The simulation experiment, as shown in Fig. 10, was repeated 20 times. The mass of a single wheat seed simulated particle was 0.0435 g.

Indoor experiment method

In order to assess the operational stability of the entire system and LabVIEW software, the coordination between the LabVIEW upper computer and the control system, the reliability of the pressure sensor operation, and the real-time performance and reliability of SPI communication, the multi-channel real-time weighing device was employed. Using a six-row wheat seeder as the experimental subject, indoor tests were conducted under the same experimental conditions to evaluate the consistency and stability of the sowing quantities for each row of the seeder. The experimental setup is depicted in Fig. 11.

On September 25, 2023, the experiments were conducted at the Agricultural Machinery and Equipment Testing Laboratory of Shandong University of Technology. The experimental equipment consisted mainly of a 6-row wheat seeder, with the groove wheel having a length of 2.5 cm and a groove wheel speed of 25 r/min, seeds in the seed box exceeding half of the box volume; a multi-channel real-time weighing device; an electromagnetic force electronic balance with an accuracy of 1×10^{-3} g; a stepper motor with a motor speed of 25 r/min; the wheat variety used for sowing was *Jimai 22*; weighing buckets; and brushes, among others.

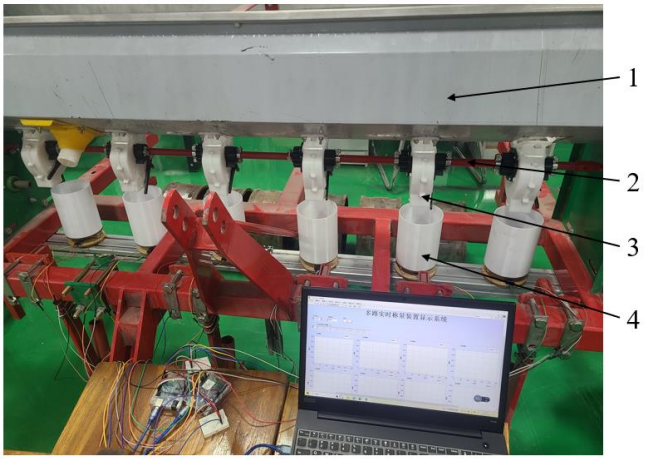

Fig. 11 - Indoor experiment

1 – seed box; 2 – propshaft; 3 – seed dispenser; 4 – weighting unit

The experiment was a static test, in which six weighing units were randomly selected from the multi-channel real-time weighing device to determine the consistency and stability of the sowing quantities for each row of the six-row wheat seeder. Prior to the start of the experiment, the stepper motor was connected to the seeding machine transmission shaft via a coupling to drive the seed dispenser for rotation. The weighing units of the multi-channel real-time weighing device were placed under each seed dispenser according to the settings from the simulation analysis. The distance between the bottom of the seeding openings and the bottom of the weighing cylinders was approximately 11 cm, designed for assessing the sowing quality of each seed dispenser. After emptying the seed box, the seeds were poured into the seed box and waited for the sowing to begin.

At the beginning of the experiment, the multi-channel real-time weighing device was started and allowed 3 seconds to stabilize before initiating the stepper motor to drive the seeder for sowing. The stepper motor ran at a speed of 25 r/min for 30 seconds, during which the multi-channel real-time weighing device displayed and recorded the experimental data. This procedure was repeated 5 times. To analyze the sowing quantity stability of each seed dispenser, the coefficient of variation for seeding stability Y_1 was used as an evaluation indicator. The sowing quality of each seed dispenser was then input into Eq. (7) for calculation.

$$\begin{cases} m_s=\frac{\sum_{i=1}^{n} m_{si}}{n} \\ Y_1=\frac{\sqrt{\frac{1}{n-1}\sum_{i=1}^{n}(m_{si}-m_s)^2}}{m_s}\cdot 100 \end{cases} \quad (7)$$

where:

m_s is average seed quality from 5 experiments (g); m_{si} is scheduled seed quality at time i (g); n is measurement times, n=5. Y_1 is the coefficient of variation for seeding stability (%).

To analyze the consistency of sowing quantities for each row of the seeder, the coefficient of variation for consistency of seeding in rows Y_2 was used as the evaluation indicator based on the sowing quality of each seed dispenser. The average sowing quantity from the 5 experiments for each seed dispenser was calculated and considered as the sowing quantity for that seed dispenser. Utilizing Eq. (8), the sowing quantity was subjected to inter-row sowing quantity consistency variation analysis.

$$Y_2=\frac{\sqrt{\frac{1}{n-1}\sum_{i=1}^{n}(m_{si}-m_s)^2}}{m_s}\cdot 100 \quad (8)$$

where:

m_s is average seed quality from six seed dispensers (g). m_{si} is seed quality from the ith dispenser (g). n is the number of dispensers, n=6. Y_2 is the coefficient of variation for consistency of seeding in rows (%).

RESULTS

Results of bench test

In order to clearly observe the changes in the absolute error, a curve depicting the changes in the absolute error was plotted, as shown in Fig. 12. The bench test experimental results are presented in Table 3.

Table 3

The bench test experimental results

Number	Absolute error 1(g)	Absolute error 2(g)	Absolute error 3(g)	Mean absolute error (g)	Mean relative error (‰)
1	0.129	0.211	0.196	0.179±0.044	6.08
2	0.216	0.133	0.114	0.154±0.054	2.67
3	0.322	0.137	0.037	0.165±0.145	1.85
4	0.305	0.087	0.291	0.228±0.122	1.97
5	0.195	0.141	0.109	0.148±0.043	1.02
6	0.300	0.244	0.242	0.262±0.033	1.48
7	0.194	0.136	0.261	0.197±0.063	0.97
8	0.103	0.300	0.192	0.198±0.099	0.86
9	0.075	0.038	0.315	0.143±0.150	0.54
10	0.147	0.205	0.121	0.158±0.043	0.49

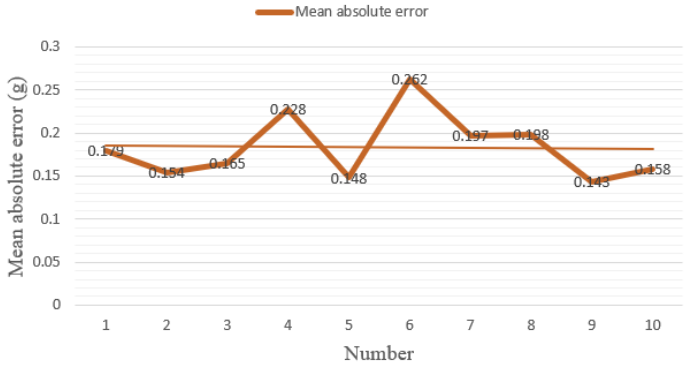

Fig. 12 - The curve of the changes in the absolute error

In the 10 sets of experimental data, the mean absolute error of the individual weighing units was randomly distributed between 0.143 g and 0.262 g, with a mean of 0.184 g. Two main factors contribute to this absolute error: the inherent error of the strain gauge pressure sensor and the impact component's force along the vertical direction during the seed's descent. The maximum and minimum mean relative errors of the weighing units are 6.08‰ and 5.4‰, respectively. As wheat seeds continue to be discharged, the mass of the wheat seeds increases, leading to a gradual reduction in the impact of absolute errors on the measurement results and an overall decreasing trend in relative errors.

Results of simulation

Analysis of collision data showed that the magnitude of the force generated in the negative Y-axis direction during collision was random, ranging from 1.508 N to 3.121 N, with a mean value of 2.220 N. The influence on the pressure sensor ranged from 0.110 g to 0.275 g, with a mean impact of 0.183 g.

The sampling frequency of the pressure sensor is 10 Hz, while the frequency at which Arduino reads sensor data is 2 Hz. When the moment of seed impact synchronizes with the data acquisition time of the pressure sensor, the impact force affects the real pressure data. As the seeds fell and accumulated, impact force simulation analyses were conducted with 500 and 1000 static seeds in the weighing cylinder, observing the changes in seed velocity to examine the process of impact force transmission, as shown in Fig. 13. In Fig. 13a, with no seed accumulation, the impact force acts directly on the bottom of the weighing cylinder. In Fig. 13b, with 500 seeds accumulated, the impact force is transmitted among the seeds, as indicated by the color of the arrows; when the impact force acts at the bottom of the cylinder, its magnitude decreases. In Fig. 13c, with 1000 seeds accumulated, the variation of impact force with time steps was observed. During the transmission of impact force, due to reasons such as inter-seed gaps and friction, the force cannot be transmitted to the bottom of the weighing cylinder.

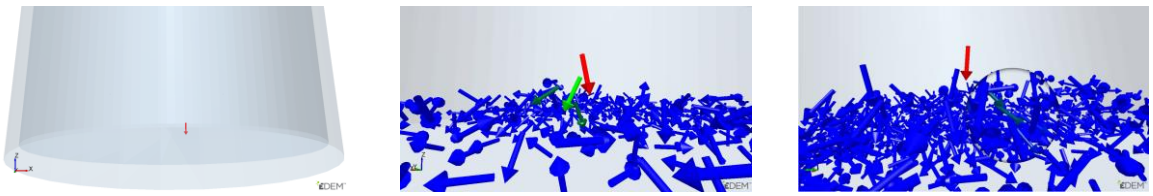

(a) (b) (c)

Fig. 13 – Process of impact force transmission

(a) With no seed accumulation; (b) With 500 seeds accumulated; (c) With 1000 seeds accumulated

Results of Indoor experiment

The experimental data results are shown in Table 4. The table includes the sowing quality data from 5 experiments for 6 seed dispensers, the calculated results of the coefficient of variation for seeding stability Y_1, and the calculated results of the coefficient of variation for consistency of seeding in rows Y_2. The calculation method for Y_1 involves taking the average of the five measurements of a single seed dispenser, computing the standard deviation of the sowing quantity for that seed dispenser, and then calculating the sowing quantity stability coefficient for the individual seed dispenser. Among the 6 seed dispensers, the maximum sowing quantity stability coefficient is 2.38%, the minimum is 0.83%, and the mean is 1.21%. The calculation method for Y_2 involves calculating the average sowing quantity from the 5 experiments for each seed dispenser, considering it as the sowing quantity for that seed dispenser, and then computing the standard deviation of the average sowing quantity for the 6 seed dispensers to determine the coefficient of variation for consistency of seeding in rows. The coefficient of variation for consistency of seeding in rows is 1.86%.

Table 4

The experimental data results

Number	Seed dispenser 1 quality(g)	Seed dispenser 2 quality(g)	Seed dispenser 3 quality(g)	Seed dispenser 4 quality(g)	Seed dispenser 5 quality(g)	Seed dispenser 6 quality(g)	Y_2 (%)
1	192.85	193.58	193.30	198.96	196.66	201.02	-
2	191.08	190.23	196.34	196.85	198.37	201.87	-
3	193.42	192.11	205.07	194.20	201.17	202.72	-
4	191.91	192.89	194.94	197.59	199.32	199.50	-
5	188.70	189.81	194.96	195.47	199.56	196.05	-
mean quality (g)	191.59	191.72	196.92	196.61	199.07	200.23	1.86
Y_1 (%)	0.96	0.86	2.38	0.94	0.83	1.31	-

As the transmission shaft of the seeder is driven by the stepper motor to rotate at a constant speed, there was no slippage of the ground wheels or shaking of the seeder. The seeders rotate synchronously at a constant speed, leading to a small value of the coefficient of variation for seeding stability. Additionally, due to the consistent groove wheel length of each seed dispenser and the uniform distribution of wheat seeds in the seed box, coupled with the small individual mass of wheat seeds, the calculation value of the coefficient of variation for consistency of seeding in rows was also relatively small.

CONCLUSIONS

(1) A multi-channel real-time weighing device has been designed that collects real-time data from various pressure sensors through Arduino controllers and displays and stores it in the LabVIEW upper computer. This device can be applied to monitor the operational quality of agricultural machinery such as row seeding, broadcast sowing, and irrigation equipment.

(2) By utilizing SPI communication, the data exchange between the master and slave Arduino boards has been achieved. In a one-master, one-slave configuration, it is possible to simultaneously collect data from 14 pressure sensors. Each slave device is an independent Arduino controller, enabling modularity that is beneficial for future expansion and improvement of functionalities. Based on the working principle of strain pressure sensors, the design of the weighing unit is reasonable, resulting in stable operation of the entire system with low production costs. This makes it easier to promote the device.

(3) The results of the bench test and indoor test demonstrate the reliability of the device, with the mean absolute error of the weighing unit ranging from 0.143 g to 0.262 g. According to simulation results, the impact of a single wheat seed on the weighing unit falls between 0.11 g and 0.275 g, with a mean impact value of 0.183 g. Under the preset test conditions, the coefficient of variation for seeding stability ranges from a maximum of 2.38% to a minimum of 0.83%, with a mean of 1.21%, while the coefficient of variation for consistency of seeding in rows was 1.86%.

ACKNOWLEDGEMENT

This research was supported by the National Natural Science Foundation of China (Grant No. 32101631 & No. 51805300), the Youth Innovation Team Project of Shandong Colleges and Universities, Science and Technology Program of Guizhou Province (QKHZDZX[2024]004) and China National Tobacco Corporation Guizhou Provincial Company Technology Project (2024520000240066).

REFERENCES

[1] Drake, T.G. (1991) Granular flow: physical experiments and their implications for microstructural theories. *Journal of Fluid Mechanics*, Vol. 225, 121-152. https://doi.org/10.1017/S0022112091001994

[2] Ding Youchun, Wang Kaiyang, Liu, Xiaodong. et al. (2021) Research progress of seeding detection technology for medium and small size seeds (中小粒径种子播种检测技术研究进展). *Transactions of the Chinese Society of Agricultural Engineering*, Vol.37:8, 30-41. https://doi.org/10.11975/j.issn.1002-6819.2021.08.004

[3] Gong Yang, Zhang Pan. (2020) Multi-channel wireless A/D acquisition system based on NRF24L01 and LABVIEW. *MATEC Web of Conferences*. Vol. 309, 01001. http://doi.org/10.1051/matecconf/202030901001

[4] Ghanbari M., Rezazadeh G. (2022) Investigating Static and Dynamic Behavior of the Strain Gauge Type Pressure Sensor in Exposure to Thermal Stresses. *Arabian Journal for Science and Engineering*, Vol.47, 8931-8944. http://doi.org/10.1007/S13369-021-06443-4

[5] Gu Tingwei, Yuan Shengjun, Gu Lin. et al. (2024) Research on dynamic calibration and compensation method of strain-gauge type force sensor. *Sensor Review*, Vol.44, No.1, 68-80. http://doi.org/10.1108/sr-08-2023-0330

[6] He Xiantao, Zhang Dongxing, Yang Li. et al. (2021) Design and experiment of a GPS-based turn compensation system for improving the seeding uniformity of maize planter. *Computers and Electronics in Agriculture*, Vol.187, p.106250. https://doi.org/10.1016/j.compag.2021.106250

[7] Karimi Hadi, Navid Hosseni, Besharati Bahram. et al. (2017) A practical approach to comparative design of non-contact sensing techniques for seed flow rate detection. *Computers and Electronics in Agriculture*. Vol.142, 164-172. https://doi.org/10.1016/j.compag.2017.08.027

[8] Li Daoliang, Yang Hao. (2018) State-of-the-art Review for Internet of Things in Agriculture (农业物联网技术研究进展与发展趋势分析). *Transactions of the Chinese Society for Agricultural Machinery*, Vol.49, 1-20. https://doi.org/10.6041/j.issn.1000-1298.2018.01.001

[9] Li Runtao, Wang Xianliang, Yao Yanchun. et al. (2022) Research on intelligent detection technology of seed planter (播种机智能检测技术研究). *Journal of Chinese Agricultural Mechanization*, Vol.43, 93-101. https://doi.org/10.13733/j.jcam.issn.2095-5553.2022.05.014

[10] Navid H., Ebrahimian S., Gassemzadeh H. R. et al. (2011) Laboratory evaluation of seed metering device using image processing method. *Australian Journal of Agricultural Engineering*, Vol.2, 1-4. https://api.semanticscholar.org/CorpusID:61725810

[11] Ramasamy, S. (2021) Sustainable Development in Agriculture Through Information and Communication Technology (ICT) for Smarter India. *International Journal of Social Ecology and Sustainable Development*, Vol.12:3, ISSN:1947-8402. https://doi.org/10.4018/IJSESD.2021070106

[12] Rossi Sebastián, Scola Ignacio Rubio, Bourges Gastón et al. (2023) Improving the seed detection accuracy of piezoelectric impact sensors for precision seeders. Part I: A comparative study of signal processing algorithms. *Computers and Electronics in Agriculture*, Vol.215, p.104449. https://doi.org/10.1016/j.compag.2023.108449

[13] Taghinezhad J., Alimardani R., Jafari A. (2013) Design a capacitive sensor for rapid monitoring of seed rate of sugarcane planter. *Agricultural Engineering International: The CIGR e-journal*, Vol.15, 23-29. https://cigrjournal.org/index.php/Ejounral/article/view/2576/1791

[14] Wu Mingliang, Yang Yang, Guan Chunyun. et al. (2014) Design and test of a control system for rapeseed metering device based on pressure sensor for seed quantity control (基于压力传感器的油菜排种量控制系统的设计与试验). *Journal of Hunan Agricultural University (Natural Sciences)*, Vol.40:5, 536-540. https://doi.org/10.13331/j.cnki.jhau.2014.05.015

[15] Wang Tongzhao, Quan Qiquan, Tang Dewei. et al. (2021) Effect of hyperthermal cryogenic environments on the performance of piezoelectric transducer. *Applied Thermal Engineering*, Vol.193, p.116725. https://doi.org/10.1016/j.applthermaleng.2021.116725

[16] Wang Weiwei, Song Lanzhou, Shi Wenbing. et al. (2024) Design and Experiment of Air-suction Double-row Staggered Precision Seed Metering Device for Maize Dense Planting (气吸双行错置式玉米密植精量排种器设计与试验). *Transactions of the Chinese Society for Agricultural Machinery*, Vol.55:3, 53-63. https://doi.org/10.6041/j.issn.1000-1298.2024.03.005

[17] Yang, B., Ding, X. W. (2012) Design of SPI bus communication in the multi-channel data acquisition systems. *Advanced Materials Research*, Vol.532, 187-191. http://doi.org/10.4028/www.scientific.net/AMR.532-533.187

[18] Yu Jiayang, Lu Caiyun, Wei Ruxue. et al. (2018) Simulation test on the performance of wheat precision seed discharger based on discrete element method (基于离散元法的小麦精量排种器性能模拟试验). *Jiangsu Agricultural Sciences*, Vol.46:8, 225-228. http://doi.org/10.15889/j.issn.1002-1302.2018.08.057

[19] Yu Qingxu, Liu Yan, Chen Xiaobing. et al. (2020) Calibration and Experiment of Simulation Parameters for Panax notoginseng Seeds Based on DEM (基于离散元的三七种子仿真参数标定与试验). *Transactions of the Chinese Society for Agricultural Machinery*, Vol.51:2, 123-132. http://doi.org/10.6041/j.issn.1000-1298.2020.02.014

[20] Zagainov Nikolay, Kostyuchenkov Nikolay, Huang Yu Xiang. et al. (2023) Line laser based sensor for real-time seed counting and seed miss detection for precision planter. *Optics and Laser Technology,* Vol.167, p.109742. http://dx.doi.org/10.1016/J.OPTLASTEC.2023.109742

[21] Zhao Baitong, Zhang Xiaohui, Kong Qingyong. et al. (2003) Current status and development trend of monitoring systems for precision seeders at home and abroad (). *Shandong Agricultural Machinery*, Vol.12, 14-16.

[22] Zhang Jicheng, Chen Haitao, Ouyang Binlin. et al. (2013) Monitoring system for precision seeders based on a photosensitive sensor (基于光敏传感器的精密播种机监测装置). *Journal of Tsinghua University (Science and Technology)*, Vol.53:2, 265-268. https://doi.org/10.16511/j.cnki.qhdxxb.2013.02.018

[23] Zhang Yang, Zhu Bin, Xie Bo. et al. (2013) Visual image and radio signal fusion identification based on convolutional neural networks. *Journal of Optics*, Vol.50, 237-244. http://dx.doi.org/10.1007/s12596-020-00672-w

[24] Zhang Xiwen, Hou Zhanfeng, Xuan Chuanzhong. (2022) Design and experiment of recognition system for coated red clover seeds based on machine vision (基于机器视觉的包衣红三叶种子识别系统的设计与试验). *INMATEH Agricultural Engineering*, Vol.66, no.1, 62-72. https://doi.org/10.35633/inmateh-66-06

[25] Zhou L.M., Niu K., Chen K.K. et al. (2022) Design and test of real-time monitoring system for non-contact fertilization flow (非接触施肥流量实时监测系统的设计与试验). *INMATEH Agricultural Engineering*, Vol.66, no.1, 351-360. https://doi.org/10.35633/inmateh-66-35